Protein Interactions in Undersaturated and Supersaturated Solutions: A Study Using Light and X-Ray Scattering

Janaky Narayanan* and X. Y. Liu†
*Department of Physics, R. J. College, Ghatkopar (W), Mumbai 400 086, India and †Department of Physics, Blk. S12, Faculty of Science, National University of Singapore, Singapore 117542

ABSTRACT Protein interactions in undersaturated and supersaturated solutions were investigated using static and dynamic light scattering and small angle x-ray scattering. A morphodrom of lysozyme crystals determined at 35°C and pH = 4.6 was used as a guideline in selecting the protein and precipitant concentrations. The osmotic second virial coefficient, B_{22}, was determined by static and dynamic light scattering. At low ionic strengths for which no crystals were formed, B_{22} was positive indicating repulsive interactions between the protein molecules. Negative B_{22} at higher ionic strengths corresponds to attractive interactions where crystallization becomes possible. At two extreme salt concentrations, small angle x-ray scattering data were collected and fitted with a statistical mechanical model based on Derjaguin–Landau–Verwey–Overbeek potential using Random Phase Approximation. This model accounted well for the small angle x-ray scattering data at undersaturated condition with constant potential parameters. At very high salt concentration corresponding to supersaturated solution this model seems to fail, possibly due to the presence of non-Derjaguin–Landau–Verwey–Overbeek hydration repulsion between the molecules.

INTRODUCTION

Understanding and predicting protein crystallization from solutions have been challenging tasks for several years (George and Wilson, 1994; Georgalis et al., 1995; Durbin and Feber, 1996; Rosenberger, 1996: Rosenberger et al., 1996; Muschol and Rosenberger, 1997; Wolde and Frenkel, 1997; Vekilov et al., 1999; Malkin et al., 1999; Neal et al., 1999; Tardieu et al., 2001). Sufficiently large single crystals are essential for understanding the structural biochemistry of proteins using x-ray Crystallography. These structural data are required for drug design and disease treatment. Protein aggregation plays an important role in several pathological conditions, such as cataract (Thomson et al., 1987; Berland et al., 1992) and sickle cell anemia (San Biagio and Palma, 1991). Slow dissolution rate of the protein crystals of narrow size distribution is used to advantage in drug delivery (Matsuda et al., 1989; Galkin and Vekilov, 2000). Apart from this, the growth of protein crystals from solution has applications in separation and purification of protein products (Curtis et al., 1998).

A large number of solution parameters that play a crucial role in deciding the crystal growth, the morphology and the quality of crystals keep protein crystallization an active field of research. Crystallization of biomolecules is a process involving nucleation and crystal growth. This process is determined to a large extent by the effective interaction between the molecules and the kinetic factors that control the nucleation and growth. The driving force for both nucleation and crystal growth is supersaturation, i.e., the concentration of solute in the solution above equilibrium solubility. Lowering temperature, increasing ionic strength, adjusting pH and increasing protein concentration can increase supersaturation. In addition, the purity of the protein and the precipitant salt and the specificity of salt also determine the kinetics and consequently crystallization.

George and Wilson (1994) demonstrated the importance of protein–protein interaction characterized by the osmotic second virial coefficient, B_{22} in protein crystallization behavior. Its value depends on the effective interaction between a pair of macromolecules in solution—a positive value reflecting predominantly repulsive interactions and a negative value indicating attractive interactions. A necessary condition for protein crystallization is that B_{22} lies in a crystallization window, $-8 \times 10^{-4} < B_{22} < -2 \times 10^{-4}$ ml mol/g^2. To determine B_{22}, techniques such as static and dynamic light scattering (George and Wilson, 1994; Muschol and Rosenberger, 1995; Rosenbaum and Zukoski, 1996; Curtis et al., 1998; Velev et al., 1998; Petsev and Vekilov, 2000), small angle neutron scattering (Gripon et al., 1997; Velev et al., 1998) and small angle x-ray scattering (Bonnete et al., 1999) are often used. Since the above scattering methods also measure the interaction parameters indirectly, one can get an insight into the interaction potentials that control the particle distribution, phase diagram, and crystallization process in macromolecular solutions. Recently Velev et al., (1998) have used static light scattering (SLS) and small angle neutron scattering to determine B_{22} and probe the interaction potentials in protein solutions at various pH and salt concentrations. The purpose of this work is to apply SLS, dynamic light scattering (DLS), and small angle x-ray scattering (SAXS) to examine systematically the conditions under which the crystallization of the model protein, lysozyme, may occur. SAXS data are collected under solution conditions of both undersaturation

Submitted May 23, 2002, and accepted for publication September 3, 2002.

Address reprint requests to Janaky Narayanan, R. J. College, Ghatkopar (W), 2/78 Krishna Mahal Pestom Sagar, Tilak Nagar P.O., Mumbai, Ma, India 400 089. Tel.: +91-22-522-4413; Fax: +91-22-522-4413; E-mail: janaky@vsnl.com.

0006-3495/03/01/523/10 $2.00

and supersaturation to evaluate the relative strengths of the interaction potentials.

Use of phase diagrams consisting of solubility curve and liquid–liquid phase transition curve is the basic strategy in selecting the solution parameters conducive to protein crystallization. In this paper, the morphodrom of the lysozyme crystals determined at 35°C and pH = 4.6 by Tanaka et al. (1996, 1997) is used to select the experimental conditions. Static and dynamic light scattering techniques are used to probe B_{22} for dilute solutions. Since the protein solubility is a direct measure of the crystal chemical potential, B_{22} for dilute solutions can be extrapolated to protein–protein interactions in the crystal. Crystallization tests by batch method are performed to elucidate the importance of the crystallization window. SAXS is used to establish the correlations between crystallization conditions. The SAXS data are fitted by a model based on Derjaguin–Landau–Verwey–Overbeek (DLVO) potential (Verwey and Overbeek, 1948), which accounts for the repulsive and attractive interactions of spherical colloidal particles. Using standard statistical mechanical models for evaluating the interparticle structure factor, $S(Q)$, the scattering intensity $I(Q)$ is calculated and fitted to obtain reasonable potential parameters from which B_{22} is calculated and compared with experimental results. Lysozyme is one of the most intensely studied proteins. The numerous parameters that decide the solution properties and the several experimental and theoretical tools available have given forth to a vast collection of data on lysozyme. Through this systematic study we revisit the intricacies of protein interactions and reinforce the notion that DLVO-based models for protein–protein interactions fail at extreme salt concentrations.

MATERIALS AND METHODS

Materials

Hen egg-white lysozyme (six times crystallized) from Seikagaku Corporation (Lot no. E99201) and sodium chloride from Merck (analytical grade) were used as received. Aqueous solutions of lysozyme and NaCl were prepared using deionized water from a Millipore Milli-Q system adjusted to a pH 4.6 ± 0.06 with 1N HCl. The solutions were filtered through 0.1 μm Anotop (Whatman) filters and mixed just before measurements. No buffer salts were used in order that the ionic strength of the solution is determined solely by the added precipitant salt (NaCl).

Methods

SLS and DLS measurements were carried out using a Brookhaven light scattering instrument with a BI9000AT correlator. He-Ne laser ($\lambda = 632.8$ nm) from Spectra Physics, Model 127 (60 mW), was used as the light source. Toluene from Aldrich (spectrophotometric grade) was used as the calibrating liquid for the determination of Rayleigh ratio, R_θ at the scattering angle $\theta = 90°$.

SAXS measurements were carried out using a Bruker AXS NanoStar instrument employing a pinhole SAXS camera, cross-coupled Göbel mirrors, and a position-sensitive area detector. A sealed x-ray tube with Cu anode (K_α wavelength of 1.542 Å) operating at 40 KV and 35 mA was used. The beam diameter at the sample was 200 μm and the sample-to-detector distance was 106.5 cm. A thermostated sample holder (±0.1°C) with a glass capillary of thickness 0.1 mm and diameter 0.78 mm was employed. The collection time was 5 h or more. The intensity recorded on a frame size of 1024 × 1024 pixels was integrated by Normalized Bin method to get a plot of $I(Q)$ versus Q where Q is the wave vector. The recorded intensity was in arbitrary unit.

Crystallization tests were carried out by batch method. The samples were loaded in 1-cm–diameter sealed test tubes and monitored for over a month. All measurements were carried out at 35.0 ± 0.1°C.

PRINCIPLES OF DATA ANALYSIS

Static light scattering

The SLS data were analyzed using the classical Zimm equation (Zimm, 1948):

$$\frac{K_0 C}{R_\theta} = \frac{1}{M_w} + 2B_{22}C, \tag{1}$$

where R_θ is the Rayleigh ratio at angle θ ($\theta = 90°$), M_w is the molecular weight of protein, and C its concentration in g/ml. The Rayleigh ratio was calculated by subtracting the solvent intensity from the solution intensity and using toluene as the standard for which $R_{90°} = 14.0 \times 10^{-6}$ cm^{-1} at $\lambda = 632.8$ nm. The constant K_0 is given by

$$K_0 = \frac{4\pi^2 n_0^2}{N_A \lambda_0^4}\left(\frac{dn}{dc}\right)^2, \tag{2}$$

where n_0 is the refractive index of the solvent, N_A is the Avogadro number, and (dn/dc) is the specific refractive index increment of the protein solution. Extrapolating the (dn/dc) values at 436 and 589 nm from the data of Huglin (1972) using a linear regression $(dn/dc) = A + B/\lambda^2$, the (dn/dc) for lysozyme at 632.8 nm was found to be 0.183 ml/g.

Dynamic light scattering

In DLS experiments, the normalized intensity autocorrelation function of the scattered light, $g^{(2)}(q,t) = \langle I(q,t)\, I(q,0)\rangle / \langle I\rangle^2$ is measured and is used to calculate the normalized time correlation function of the scattered electric field, $g^{(1)}(q,t) = \langle E^*(q,t)\, E(q,0)\rangle / \langle E\rangle^2$.

For a Gaussian signal, the Seigert relation, $g^{(2)}(q,t) = 1 + f\,|g^{(1)}(q,t)|^2$ holds, where the coherence factor, f, measures the degree of coherence of the scattered light (Berne and Pecora, 1976). Here, q is the wave vector given by

$$q = \frac{4\pi n_0}{\lambda}\sin(\theta/2), \tag{3}$$

where θ is the scattering angle. For monodisperse, rigid, globular scatterers, $g^{(1)}(q,t) = \exp(-\Gamma t)$, Γ being the decay or the relaxation rate. $\Gamma = D_m q^2$, where D_m is the mutual diffusion coefficient which is concentration dependent. For dilute solutions (Brown and Nicolai, 1993),

$$D_m(C) = D_o(1 + k_d C). \tag{4}$$

The parameter D_o is related to R_H, the hydrodynamic radius and η, the solvent viscosity through Stokes-Einstein equation,

$$D_o = \frac{k_B T}{6\pi\eta R_H}. \quad (5)$$

The parameter k_d can be expressed as

$$k_d = 2M_w B_{22} - k_f - 2\upsilon, \quad (6)$$

where k_f is the coefficient of the linear term in the development of the friction coefficient factor and υ is the partial specific volume of the protein molecule. k_f can be determined from self-diffusion measurements using pulsed-gradient, spin-echo (PGSE) NMR. Selecting a linear correlator of 200 channels, the correlation decay was monitored from 5 μs to 1 ms averaged over 2 min duration. The scattering angle was 90°.

Small angle x-ray scattering

In the absence of multiple scattering, for an ensemble of particles uniformly dispersed in a medium, the measured scattered intensity $I(Q)$ is proportional to the differential scattering cross section per unit volume, i.e., $d\Sigma/d\Omega$, which is given by Orthaber et al. (2000),

$$\frac{d\Sigma(Q)}{d\Omega} = C(\Delta\rho)^2\upsilon^2 M_1 P(Q)S(Q), \quad (7)$$

where C is the concentration of the solute (g/cm^3), M_1 is the mass of one particle, $P(Q)$ is the form factor, $S(Q)$ is the structure factor, and $\Delta\rho$ is the excess scattering length density (cm^{-2}) given by

$$\Delta\rho = \frac{1}{V_1}\sum_j b_j - \rho_s. \quad (8)$$

The volume of a single particle is V_1; the scattering length density of the solvent is ρ_s and $\sum_j b_j$ is the sum of the scattering lengths of all the constituent atoms forming the particle. In x-ray scattering, the scattering length b of an atom is proportional to the atomic number Z and is given by $b = Zr_o$, where r_o is the classical electron radius $= 2.82 \times 10^{-13}$ cm.

The form factor $P(Q)$ depends on the shape and size of the particles. For spherical particles,

$$P(Q) = [3j_1(QR)/(QR)]^2, \quad (9)$$

where $j_1(x) = (\sin x - x\cos x)/x^2$, is the first-order spherical Bessel function, R is the radius of the particle, and Q is the wave vector, which for a scattering angle θ, is given by

$$Q = \frac{4\pi}{\lambda}\sin(0/2). \quad (10)$$

Various statistical mechanical models derived from liquid state theories (Croxton, 1975; Hansen and McDonald, 1976) are used in the calculation of the interparticle structure factor $S(Q)$ for colloidal particles (Belloni, 1991; Kaler, 1995).

$$S(Q) = [1 - nc(Q)]^{-1}, \quad (11)$$

where n is the particle number density and $c(Q)$ is the Fourier transform of the direct correlation function $c(r)$, which has approximately the same range as that of interparticle potentials. For short-ranged (hard-sphere) potentials, the Percus-Yevick (PY) approximation is used. This applies to uncharged particle dispersions or short-chain polymeric species, which are sterically stabilized. For ionic systems, the Hypernetted Chain approximation is more suitable. But the solution of the Ornstein-Zernike equation (Hansen and McDonald, 1976) that is required to obtain $S(Q)$ can be obtained only numerically. The Hypernetted Chain integral equation method is more reliable to study all correlations in polyelectrolyte solutions using n-component primitive model (Belloni, 1991). Rescaled mean spherical approximation, which gives analytical solution, is well suited in the case of highly charged ionic systems showing structural ordering (Hayter and Penfold, 1981, Hansen and Hayter, 1982). Since the PY approximation does not predict a phase transition due to lack of attractive tail in the potential, the Sticky-Hard Sphere model, also called Baxter model, is used (Baxter, 1968). For moderately charged systems in which the charge can be continuously tuned by additives, the random phase approximation (RPA) can be used (Grimson, 1983; Grimson et al., 1991; Manohar and Kelkar, 1992, Kelkar et al., 1992). In this method, the reference system is either hard-sphere or sticky hard-sphere potential and the other interactions, generally given in the form of DLVO potential, i.e., sum of attractive and repulsive contributions, are treated as a perturbation. Under RPA, the structure factor, $S(Q)$ is given by Hansen and McDonald (1976),

$$S(Q) = S_0(Q)[1 + \beta n S_0(Q)V'(Q)]^{-1}, \quad (12)$$

where $S_0(Q)$ is the structure factor of the reference system and $V'(Q)$ is the Fourier transform of the perturbation potential, $V(r)$. The perturbation must be sufficiently low; i.e., $\beta n S_0(Q)V'(Q) < 1$ for all Q-values. Here $\beta = 1/(k_B T)$, k_B being the Boltzmann constant.

For globular proteins in moderate to high salt concentrations, the interparticle interaction energy V_{22} can be expressed as (Curtis et al., 1998):

$$V_{22}(r) = V_{HS}(r) + V_C(r) + V_A(r) + V_o(r) + V_a(r), \quad (13)$$

where r is the center-to-center separation of the particles. The hard-sphere (excluded-volume) potential V_{HS} (r) is given by

$$\begin{aligned} V_{HS}(r) &= \infty \quad \text{for } r < \sigma \\ &= 0 \quad \text{for } r > \sigma, \end{aligned} \quad (14)$$

with σ being the diameter of the particle. V_C is the screened Coulomb potential given by Verwey and Overbeek (1948):

$$V_C(r) = \frac{Z^2e^2}{\varepsilon(1+0.5\kappa\sigma)^2}\frac{\exp[-\kappa(r-\sigma)]}{r} \quad (15)$$

Ze is the charge on the particle, ε is the dielectric constant of the medium, and κ is the reciprocal Debye-Huckel screening length that decides the range of the interaction.

$$\kappa^2 = \frac{4\pi e^2}{\varepsilon k_B T}\sum_i n_{io}Z_i^2 = \frac{8\pi e^2 N_A I}{10^3 \varepsilon k_B T} \quad (16)$$

n_{io} is the mean density of ions of type i having charge Z_i and I is the ionic strength of the solution. At 300 K, $\kappa^{-1} = 3/\sqrt{I}$ Å. The van-der-Waals potential is given by Verwey and Overbeek (1948):

$$V_A(r) = \frac{-A}{12}\left[\frac{\sigma^2}{r^2-\sigma^2} + \frac{\sigma^2}{r^2} + 2ln\left(\frac{r^2-\sigma^2}{r^2}\right)\right]. \quad (17)$$

A is the Hamaker constant (in k_BT) determined by the material properties of the particles and the dispersion medium. V_o in Eq. 13 is the osmotic attractive potential due to excluded-volume effect of the salt ions and V_a is the square-well potential that accounts for self-association of proteins. V_{HS}, V_C, and V_A are described by DLVO potential. At low salt concentrations, the osmotic attractive potential is not important. At high salt concentrations, the contributions from the attractive potentials V_A and V_o far exceed the repulsive Coulomb interaction, V_C (Curtis et al., 1998). Since the net force is the sum of the repulsive and the attractive contributions, we assume that it can be treated as a perturbation to apply RPA. Also, for the concentrations used in this study, the number density of lysozyme molecules is low. Assuming a spherical diameter σ of 36 Å, the volume fraction of lysozyme used in this study, $\eta = \pi\sigma^3 n/6$ is in the range 0.04–0.082. Thus,

$$S(Q) = S_0(Q)[1 + \beta n S_0(Q)\{V_{AY}(Q) + V_C(Q)\}]^{-1}. \quad (18)$$

In the above equation, $V_{AY}(Q)$ is the Fourier transform of the sum of the attractive potentials, V_A and V_o, which is modeled in the form of a Yukawa-type potential, $V_{AY}(r)$:

$$V_{AY}(r) = -J\left(\frac{\sigma}{r}\right)\exp\left[\frac{-(r-\sigma)}{d}\right], \quad (19)$$

where J in k_BT is the depth of attractive potential at contact ($r = \sigma$) and d, its range. Malfois et al. (1996) and Tardieu et al. (1999) have used a similar potential to characterize the attractive van-der-Waals potential to explain their SAXS data on lysozyme solutions.

The hard-sphere reference system under PY approximation is approximated by a rectangular empty-core function of depth given by Croxton (1975) and Kelkar et al. (1992):

$$c_{ec}(r) = c_{PY\ at\ r=\sigma} = \frac{\eta(3-\eta^2)-2}{2(1-\eta)^4}. \quad (20)$$

Hence,

$$[S_0(Q)]^{-1} = 1 - nc_{ec}(Q) = 1 - \frac{12\eta[\eta(3-\eta^2)-2]}{(1-\eta)^4}\frac{j_1(Q\sigma)}{Q\sigma}. \quad (21)$$

From Eqs. 15, 18, 19, and 21, $S(Q)$ can be evaluated. Since the scattered intensity has not been calibrated on absolute scale, the equation,

$$I(Q) = K\frac{d\Sigma(Q)}{d\Omega} = KC(\Delta\rho)^2 v^2 M_1 P(Q)S(Q) \quad (22)$$

was used to fit the measured intensity taking K as a fitting parameter. The other potential parameters used in the fitting are the charge on lysozyme molecule, Z, and the depth and range of the attractive potential, J and d, respectively. The radius of the lysozyme molecule was fixed at its hydrodynamic radius of 18 Å by approximating the prolate ellipsoidal structure (45 Å × 30 Å × 30 Å) to an equivalent sphere of radius 17.2 Å and allowing for a hydration layer thickness ~0.8 Å (Georgalis et al., 1993).

RESULTS AND DISCUSSION

Two regions of protein concentrations were selected as per the morphodrom of lysozyme crystals evaluated by Tanaka et al. (1996, 1997)—dilute region (1.5–12 mg/ml) and concentrated region (40–80 mg/ml). Up to an NaCl concentration of ~1 wt %, no crystal growth is expected for the entire range of protein concentration (0–100 mg/ml). Above 1 wt %, the NaCl concentration required for crystallization increases with decreasing protein concentration. SLS and DLS studies were performed within the dilute region of lysozyme concentration in the presence of NaCl concentration of 0.05–7.5 wt % to minimize the interference from higher order terms in the virial expansion and concentration-induced protein aggregation. For crystallization tests three high concentrations of lysozyme of 40, 60, and 80 mg/ml were selected in the presence of 0.05, 0.2, 2.5, and 5 wt % NaCl. SAXS data were collected for these lysozyme concentrations in the presence of 0.05 and 5 wt % NaCl.

Static light scattering

Fig. 1 shows a plot of K_0C/R_θ against the lysozyme concentration, C, at pH 4.6 ± 0.06 and temperature 35 ± 0.1°C. As per Eq. 1, the intercept corresponds to reciprocal molecular weight of lysozyme. The data do not collapse at a single point on the ordinate axis as expected. The dispersion in the intercepts notwithstanding, the average molecular weight is estimated to be 14,130, close to the value

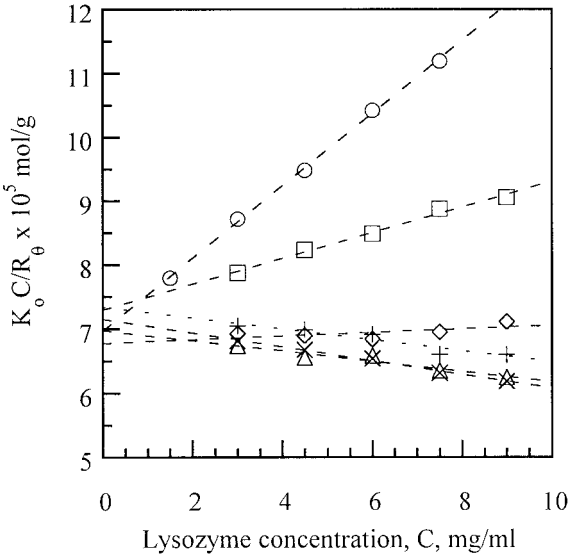

FIGURE 1 Plot of SLS data according to Eq. 1 for different salt concentrations in wt %: 0.05 (*circles*), 0.2 (*squares*), 0.75 (*diamonds*), 2.5 (*times*), 5 (*pluses*), and 7.5 (*triangles*).

found in the literature (14,300). The virial coefficients obtained from the slopes are plotted against NaCl concentration in Fig. 2. As expected from the morphodrom of Tanaka et al. (1996, 1997), for [NaCl] $<$ 1 wt %, B_{22} is positive indicating that the protein-protein interaction is predominantly repulsive and not conducive to crystal formation. For higher salt concentrations, B_{22} values are all negative and within the crystallization window.

Dynamic light scattering

The findings of SLS studies on the sign of B_{22} and its correlation to crystallization were verified by measuring the mutual diffusion coefficient, D_m, of the lysozyme molecules in the dilute region of protein concentration. The results are plotted in Fig. 3. The mutual diffusion coefficient values, D_m, for pure lysozyme found in this study are much larger than that reported by other authors (Eberstein et al., 1994; Muschol and Rosenberger, 1995; Valstar et al., 1999). The reason for this can be twofold—1. the temperature of the present study is much higher (35°C) and 2. inasmuch as no buffer salts are used, the repulsive force can be much larger in magnitude due to lack of screening. The positive slopes for [NaCl] = 0 and 0.75 wt % suggest that B_{22} is positive for these concentrations (compare to Eqs. 4 and 6). The negative slope for [NaCl] = 7.5 wt % indicates a negative B_{22} and a resultant attractive force between the lysozyme molecules. The mean hydrodynamic radius, R_H of 17.8 Å, evaluated from the intercepts D_o using Eq. 5 agrees well with the values reported in the literature (Skouri et al., 1992; Muschol and Rosenberger, 1995; Valstar et al., 1999).

Recently Price et al. (1999) have measured the self-diffusion coefficient of lysozyme using PGSE NMR at various pH, temperature, and protein and salt concentrations to elucidate the solution and aggregation properties. The diffusion measurements performed at 25°C and pH 4.6 on lysozyme concentration up to 5 mM (~75 mg/ml) in the presence of 0, 0.15, and 0.5 M NaCl showed that in the absence of salt there was apparently no aggregation taking place. In the presence of salt, the diffusion coefficients decreased more quickly with increasing lysozyme concen-

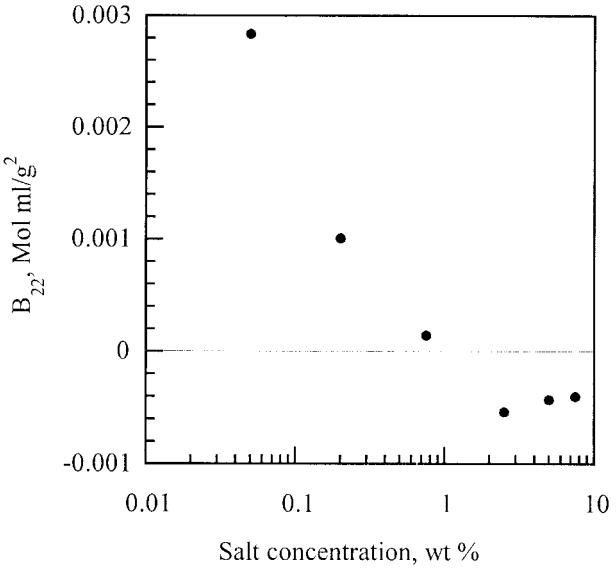

FIGURE 2 Variation of osmotic second virial coefficient with salt concentration.

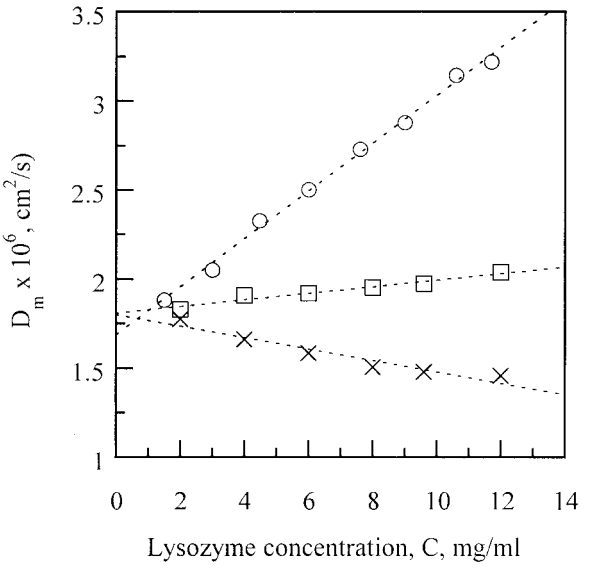

FIGURE 3 Plot of the mutual diffusion coefficient of the lysozyme molecules against lysozyme concentration for different salt concentrations in wt %: 0 (*circles*), 0.75 (*squares*), and 7.5 (*times*). Dotted lines are linear fits to Eq. 4.

trations and the data could be fitted only with models accounting for the presence of higher oligomeric states. The DLS experiments also give a similar result, namely, the mutual diffusion coefficients decrease sufficiently in the presence of salt suggesting increased attraction and possible aggregation of the lysozyme molecules. However, whereas Price et al. (1999) have reported a negative slope for the variation of self-diffusion coefficient with lysozyme concentration in the absence of salt, the DLS experiments (this article; Eberstein et al., 1994; Muschol and Rosenberger, 1995; Valstar et al., 1999) give a positive slope for the variation of mutual diffusion coefficient. The lysozyme solutions used in the study by Price et al. (1999) are crowded systems with a high probability for the lysozyme molecules to collide numerous times during the diffusion measurements. Hence the measured self-diffusion coefficient is expected to decrease due to self-obstruction as the lysozyme concentration increases.

Crystallization

The crystallization tests corroborated with the findings of SLS and DLS studies on B_{22}. For all lysozyme concentrations studied (40, 60, and 80 mg/ml), there was no crystal growth observed over a month for NaCl concentrations of 0.05 wt % and 0.2 wt %. In samples containing 5 wt % NaCl, on visual observation, spherulitic crystal growth was seen in 10 h for 80-mg/ml, 22 h in 60-mg/ml, and 44 h in 40-mg/ml lysozyme concentrations. The crystal growth was rapid and dense for the 80-mg/ml sample. The morphology of the spherulitic species was similar to that observed by Chow et al. (2002) in our laboratory, by placing the protein–precipitant mixture in the middle of two layers of immiscible oils and monitoring the time evolution of spherulites using transmitted polarizing microscopy. For [NaCl] = 2.5 wt %, the crystal growth was slow and first crystals were observed within 6–15 days after the sample preparation. In these samples single crystals grew with a morphology resembling the orthorhombic rectangular crystals reported by Tanaka et al. (1996, 1997).

Small angle x-ray scattering

Based on the results of the crystallization tests, we selected two extreme salt concentrations, namely, 0.05 wt % and 5 wt % for SAXS study. The former corresponds to undersaturation and the latter supersaturation conditions for the selected lysozyme concentrations. The data were collected for 8 h in the case of [NaCl] = 0.05 wt % and 5 h in the case of [NaCl] = 5 wt %. The transmissions of the protein samples, τ, were determined using Glassy Carbon as standard and the electrolyte solution as background. The solvent subtracted intensity was calculated from

$$I(Q) = I_p(Q) - \tau I_s(Q), \tag{23}$$

where $I_p(Q)$ and $I_s(Q)$ are respectively the scattered intensity for protein solution and solvent. The intensities normalized to baseline are plotted in Figs. 4 and 5. The scattered intensity recorded for 0.05 wt % NaCl concentration (Fig. 4) shows strong correlation peaks and a dip at zero-Q region, which suggest the presence of predominantly repulsive interaction leading to structural ordering. In the case of [NaCl] = 5 wt %, the intensity increases monotonically toward zero-Q indicating predominantly attractive interactions (Fig. 5). These observations are well recorded in several ionic micellar

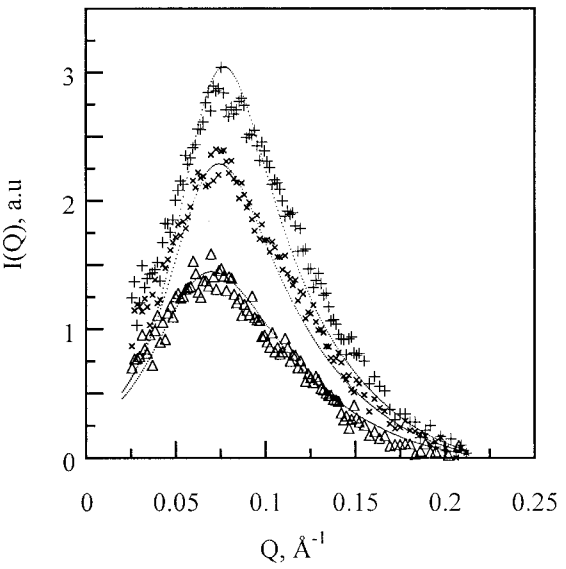

FIGURE 4 Plot of SAXS intensity in arbitrary unit against wave vector for different lysozyme concentrations in mg/ml: 80 (*pluses*), 60 (*times*), and 40 (*triangles*). The dotted lines are theoretical fits using Eq. 22. The fitting parameters are given in Table 1. The salt concentration is 0.05 wt %.

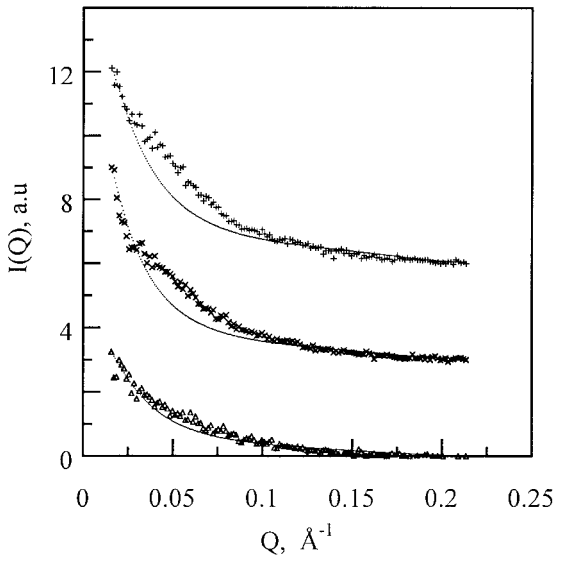

FIGURE 5 Plot of SAXS intensity in arbitrary unit against wave vector for different lysozyme concentrations in mg/ml: 80 (*pluses*), 60 (*times*), and 40 (*triangles*). The dotted lines are theoretical fits using Eq. 22. The fitting parameters are given in Table 1. The salt concentration is 5 wt %. The ordinates of successive curves are shifted by three units for clarity.

systems in the presence of salt (Bendedouch et al., 1983; Kelkar et al., 1991; Goyal et al., 1991).

The SAXS intensity was calculated using Eq. 22. For the calculation of excess scattering length density of lysozyme over solvent, $\Delta\rho$, the following data from Orthaber et al. (2000) were used: the number of electrons in protein molecule $= 3.22 \times 10^{23}$ *e*/*g* and partial specific volume of lysozyme, $\upsilon = 0.756$ cm^3/*g*. The scattering length density of the solvent was calculated taking into account the electrolyte concentration. A value of $M_w = 14{,}300$ for molecular weight was assumed to calculate $M_1 = M_w / N_A$. The form factor $P(Q)$ was calculated from Eq. 9 assuming the radius of the lysozyme molecule to be 18 Å. The structure factor $S(Q)$ was calculated as explained under data analysis using Eqs. 15, 18, 19, and 21.

In Fig. 4, the calculated SAXS intensity for the three lysozyme concentrations in the presence of [NaCl] = 0.05 wt % (8.6 mM) are plotted. The fittings seem to be reasonably good. As noted by Tardieu et al. (1999), though at the pH value of 4.6 used in this study the charge on protein is expected to be ~10 (Tanford and Roxby, 1972), the data could be fitted with only a much smaller value of $Z = 6$. The attractive potential is found to have a depth $J = 3\ k_BT$ and range $d = 3$ Å, which conforms to the findings of Tardieu et al. (1999). Since the salt concentration is quite low, the contribution to the attractive potential $V_{AY}(r)$ is mostly from the van-der-Waals force with little contribution from the osmotic attractive potential, $V_o(r)$ (Curtis et al., 1998). Hence $J = 3\ k_BT$ compares well with the theoretical value of the Hamaker constant, A (Tardieu et al., 1999). For all the three protein concentrations, the data could be fitted with the same values of Z, J, and d, but with minor variations in the instrument calibration constant, K, as shown in Table 1. Thus for very low salt concentrations, the DLVO potential comprising the hard core repulsion, screened Coulomb repulsion and van-der-Waals attraction explains the SAXS data quite well.

Being amphoteric, individual protein molecules in solution are in equilibrium with H^+ and the net surface charge carried by a protein macro-ion is largely determined by the pH of the solution. In lysozyme molecule, the charged groups are symmetrically distributed on the surface (Barlow and Thornton, 1986). Tanford and Roxby (1972) have determined the average charge on a lysozyme macro-ion in aqueous solution as a function of pH from hydrogen-ion titration. Lysozyme macro-ions in solution are known to readily complex Cl^- (Steinhardt and Renolds, 1969). The anion adsorption can lower the net charge on the protein below that estimated from hydrogen-ion titration for pH $<$ *pI*. Curtis et al. (1998) have estimated the number of Cl^- ions bound to the lysozyme at various pH from the regressed net charge obtained while fitting the experimental B_{22} values and the charge due to the hydrogen-ion equilibria. Eberstein et al. (1994) have investigated the molecular interactions in crystallizing lysozyme solutions using DLS and DLVO potential. They obtained $Z = 6.4$ and $A = 7.7\ k_BT$ as the fitting parameters to explain the mutual diffusion coefficient of lysozyme molecules in the presence of NaCl of widely varying concentrations at pH = 4.2. However, Muschol and Rosenberger (1995) have reported the values to be $Z = 10.7$ and $A = 8.1\ k_BT$ in a similar study. Eberstein et al. (1994) have used an expression for a screened Coulomb potential that is different from Eq. 15 and applicable for $\kappa\sigma/2 > 2.5$ (Verwey and Overbeek, 1948). Muschol and Rosenberger (1995) have used a lower cutoff of 0.18 nm for the surface separation (r-σ) of the macro-ions in the expression for the screened Coulomb potential (Eq. 15) and van-der-Waals potential. This lower cutoff, which accounted for the thickness of Stern layer, was found to have considerable impact on the fitting results. Thus under similar solution conditions, different fitting results are reported in the literature for the net protein charge, Ze, and the Hamaker constant, A, suggesting the importance of the choice of parameterization in the DLVO potential.

TABLE 1 Fitting parameters for SAXS data

Lysozyme conc., C (mg/ml)	[NaCl] = 0.05 wt %			[NaCl] = 5 wt %		
	K	J (k_BT)	d (Å)	K	J (k_BT)	d (Å)
40	5.35	3	3	3.2	10	3.8
60	5.45	3	3	3.4	9	3.5
80	5.25	3	3	3.5	8	3.3

The parameters: instrument calibration constant, K, and the depth and range of the attractive potential, J and d, respectively (compare to Eqs. 19 and 22), obtained for fitting the SAXS intensity for various lysozyme concentrations and two extreme values of salt concentrations. The other two parameters, namely, the radius and charge on the lysozyme molecules, were kept constant at R = 18 Å and Z = 6, respectively.

The set of data shown in Fig. 5 are for a high salt concentration of 5 wt % (860 mM). At this salt concentration, as mentioned earlier, the crystal growth is rapid. Hence the collection time was reduced to 5 h compared to 8 h for the set of data for low salt. Nevertheless, nucleation of protein molecules leading to crystal growth cannot be ruled out in these samples especially for higher lysozyme concentrations. It is not clear if the small humps seen in Fig. 5 in $I(Q)$ for a Q-range of 0.03–0.08 Å^{-1} can be attributed to nucleation and growth of crystals. The ordinates of successive curves have been shifted by three units for clarity. The data fitting was found to be insensitive to variations in Z due to the large screening effect of the salt, suggesting negligible repulsive Coulomb interaction. Considering the attractive potentials, the Hamaker constant, A (compare to Eq. 17), depends on the index of refraction of the medium in which the protein is dissolved (Israelachvili, 1992) and the index of refraction increases approximately linearly with increasing ionic strength (Broide et al., 1996). This can account for a small increase in the value of A at high ionic strengths and consequent increase in the van-der-Waals attractive in-

teraction, $V_A(r)$. The contribution to attractive potential by $V_o(r)$ due to osmotic excluded volume effect of salt ions will also be quite high (Curtis et al., 1998). Hence the strength and range of attractive interaction, $V_{AY}(r)$ (compare to Eq. 19), which is the resultant of $V_A(r)$ and $V_o(r)$, can increase at high salt concentration. The potential parameters obtained by fitting the experimental SAXS data are listed in Table 1. The difference in the calibration constant, K, can be attributed to the change of sample cell used for the two sets of data.

Curtis et al. (1998) have discussed the relative contributions of $V_C(r)$, $V_A(r)$, and $V_o(r)$ to the net interaction potential of ovalbumin for two extreme salt concentrations. Our results are in accordance with their findings. However, in the following we show that though at high salt concentrations the inclusion of $V_o(r)$, the osmotic excluded volume effect of salt ions in the DLVO potential can justify the enhancement of the attractive forces, it fails to account correctly for the forces that contribute to B_{22}. Using the same potential parameters obtained in the determination of SAXS intensity, B_{22} was calculated from

$$B_{22} = \frac{N_A}{2M_w^2}\int_0^\infty \left[1 - \exp\left(\frac{-V_{22}(r)}{k_B T}\right)\right] 4\pi r^2 dr, \qquad (24)$$

where

$$V_{22}(r) = V_{HS}(r) + V_C(r) + V_{AY}(r). \qquad (25)$$

In the case of [NaCl] = 0.05 wt %, the calculated B_{22} was 3.47×10^{-3} mol ml/g^2 which agrees well with the experimental value of 2.84×10^{-3} mol ml/g^2, obtained from SLS studies. However, the mean calculated value of B_{22} of -6.9×10^{-2} mol ml/g^2 in the case of [NaCl] = 5 wt % was in total disagreement with the experimental value of -4.28×10^{-4} mol ml/g^2, obtained from SLS studies, suggesting that the attractive potential parameter J is overestimated by the model.

Thus the DLVO potential consisting of a combination of an attractive potential (dominantly van-der-Waals) and repulsive Coulomb potential with constant potential parameters seems to account correctly for the scattered intensity recorded in this study at low ionic strength. However, at high salt concentration, this model potential seems to fail. Velev et al. (1998) have reported a large discrepancy between theory and experiment at low electrolyte concentration while using DLVO type model. The failure of DLVO potential to explain the salt dependence of the protein data has been reported by several other authors—Broide et al. (1996) in the case of lysozyme, Petsev and Vekilov (2000) in the case of apoferritin, and Molina-Bolivar et al. (1997) in the case of immunoglobulin-polymer system. These authors attributed the anomalous stability at high salt concentrations observed in these systems to the existence of hydration repulsion resulting from the hydrated counterions adsorbed on the protein. This repulsive force is shown to dominate at short range (Molina-Bolivar et al., 1997), when the double layer is compressed due to high ionic strength. This warrants an extended DLVO theory, which includes the repulsive hydration force that can explain the experimental data at high ionic strengths. The DLVO model is also unable to resolve short-range orientational interactions (Velev et al., 1998; Neal et al., 1999), salt specificity of Hofmeister series (Muschol and Rosenberger, 1995; Curtis et al., 1998; Tardieu et al., 1999), and other specific effects where chemical composition intervenes (Malfois et al., 1996). Our work underlines the need for the hydration and other specific forces to be well understood and quantified to account for the protein data at extreme salt concentrations.

CONCLUSIONS

We investigated protein–protein interactions in undersaturated and supersaturated solutions using static and dynamic light scattering and small angle x-ray scattering. The model protein lysozyme in the presence of the precipitant, sodium chloride, was used in this study. The morphodrom of lysozyme crystals determined at 35°C and pH = 4.6 by Tanaka et al. (1996, 1997) was used as the guideline in selecting the protein and precipitant concentrations. At low electrolyte concentrations corresponding to the undersaturation conditions, the osmotic second virial coefficient, B_{22}, determined by SLS and DLS was positive indicating repulsive protein–protein interaction that inhibits crystallization. At high salt concentrations for which crystal formation has been confirmed experimentally, B_{22} was negative and within the crystallization window suggested by George and Wilson (1994). SAXS measurements were performed at extreme salt concentrations selected in this study, namely, 0.05 wt % (8.6 mM) and 5 wt % (860 mM). The SAXS data were fitted with a statistical mechanical model based on DLVO potential which accounts for the repulsive and attractive interactions of spherical colloidal particles. The hard-sphere potential was taken as reference system. The repulsive screened Coulomb interaction and an attractive Yukawa type potential were treated as perturbation in RPA. The attractive Yukawa type potential included the van-der-Waals interaction and the osmotic-attractive potential due to excluded-volume effect of the salt ions. This model accounted well for all the SAXS data at undersaturation condition with constant potential parameters. The B_{22} value calculated with these potential parameters agreed well with the experimental result. However, at very high salt concentration, the depth of the attractive potential was overestimated and the calculated B_{22} was in total disagreement with the experimental value. The screened Coulomb interaction becomes negligible at very high ionic strength for short ranges due to the compression of the double layer. As suggested by several authors, the repulsive hydration interactions must be playing a predominant role at high

ionic strength, which warrants a quantitative formulation of extended DLVO potential that includes the hydration forces in the repulsive component.

We are thankful to Dr. C. Manohar, Dr. Kurt Erlacher, Dr. Bruce Weiner, Dr. Prashant Sawant, and Ms. Lim Tzu-Lin Adele for discussions. Technical assistance by Mr. Teo Hoon Hwee and Mrs. Tan Teng Jar is acknowledged.

J.N. expresses her gratitude for a Visiting Senior Research Fellowship awarded by the National University of Singapore.

REFERENCES

Barlow, D. J., and J. M. Thornton. 1986. The distribution of charged groups in proteins. *Biopolymers*. 25:1717–1733.

Baxter, R. J. 1968. Percus-Yevick equation for hard spheres with surface adhesion. *J. Chem. Phys*. 49:2770–2774.

Belloni, L. 1991. Interacting monodisperse and polydisperse spheres. *In* Neutron, X-Ray and Light Scattering. P. Lidner and T. Zemb, editors. Elsevier Science, Amsterdam. 135–155.

Bendedouch, D., S. H. Chen, and W. C. Koehler. 1983. Determination of interparticle structure factors in ionic micellar solutions by small angle neutron scattering. *J. Phys. Chem*. 87:2621–2628.

Berland, C. R., G. M. Thurston, M. Kondo, M. L. Broide, J. Pande, O. Ogun, and G. B. Benedek. 1992. Solid–liquid phase boundaries of lens protein solutions. *Proc. Natl. Acad. Sci. USA*. 89:1214–1218.

Berne, B. J., and R. Pecora. 1976. Dynamic Light Scattering. Wiley, New York.

Bonnete, F., S. Finet, and A. Tardieu. 1999. Second virial coefficient: variations with lysozyme crystallization conditions. *J. Crystal Growth*. 196:403–414.

Broide, M. L., T. M. Tominc, and M. D. Saxowsky. 1996. Using phase transitions to investigate the effect of salts on protein interactions. *Phys. Rev. E*. 53:6325–6335.

Brown, W., and T. Nicolai. 1993. Dynamic properties of polymer solutions. *In* Dynamic Light Scattering—The Method and Some Applications. W. Brown, editor. Clarendon Press, Oxford. 272–317.

Chow, P. S., J. Zhang, X. Y. Liu, and R. B. H. Tan. 2002. Spherulitic growth in protein solutions. *Int. J. Mod. Phys. B*. 16:354–358.

Croxton, C. A. 1975. Introduction to Liquid State Physics. John Wiley & Sons, London.

Curtis, R. A., J. M. Prausnitz, and H. W. Blanch. 1998. Protein–protein and protein–salt interactions in aqueous protein solutions containing concentrated electrolytes. *Biotechnol. Bioeng*. 57:11–21.

Durbin, S. D., and G. Feber. 1996. Protein crystallization. *Annu. Rev. Phys. Chem*. 47:171–204.

Eberstein, W., Y. Georgalis, and W. Saenger. 1994. Molecular interactions in crystallizing lysozyme solutions studied by photon correlation spectroscopy. *J. Crystal Growth*. 143:71–78.

Galkin, O., and P. G. Vekilov. 2000. Are nucleation kinetics of protein crystals similar to those of liquid droplets? *J. Am. Chem. Soc*. 122: 156–163.

Georgalis, Y., A. Zouni, W. Eberstein, and W. Saenger. 1993. Formation dynamics of protein precrystallization fractal clusters. *J. Crystal Growth*. 126:245–260.

Georgalis, Y., J. Schuler, J. Frank, M. D. Soumpasis, and W. Saenger. 1995. Protein crystallization screening through scattering techniques. *Adv. Colloid Interface Sci*. 58:57–86.

George, A., and W. W. Wilson. 1994. Predicting protein crystallization from a dilute solution property. *Acta Crystallogr. D*. 50:361–365.

Goyal, P. S., B. A. Dasannacharya, V. K. Kelkar, C. Manohar, K. Srinivasa Rao, and B. S. Valaulikar. 1991. Shapes and sizes of micelles in CTAB solutions. *Physica B*. 174:196–199.

Grimson, M. J. 1983. Small-angle scattering from colloidal dispersions. *J. Chem. Soc., Faraday Trans 2*. 79:817–832.

Grimson, M. J., I. L. McLaughlin, and M. Silbert. 1991. On the stability of charge-stabilized colloidal dispersions. *J. Phys. Condens. Matter*. 3:7995–8003.

Gripon, C., L. Legrand, I. Rosenman, O. Vidal, M. C. Robert, and F. Boue. 1997. Lysozyme–lysozyme interactions in under- and super-saturated solutions: a simple relation between the second virial coefficients in H_2O and D_2O. *J. Crystal Growth*. 178:575–584.

Hansen, J. P., and I. R. McDonald. 1976. Theory of Simple Liquids. Academic Press, London.

Hansen, J. P., and J. B. Hayter. 1982. A rescaled mean spherical approximation structure factor for dilute charged colloidal dispersions. *Mol. Phys*. 46:651–656.

Hayter, J. B., and J. Penfold. 1981. An analytic structure factor for macroion solutions. *Mol. Phys*. 42:109–118.

Huglin, M. B. 1972. Specific refractive index increments. *In* Light Scattering from Polymer Solutions. M. B. Huglin, editor. Academic Press, New York.

Israelachvili, J. 1992. Intermolecular and Surface Forces. Academic Press, San Diego.

Kaler, E. W. 1995. Small-angle scattering from complex fluids. *In* Modern Aspects of Small-Angle Scattering, NATO ASI Series C, Vol. 451. H. Brumberger, editor. Kluwer Academic, Dordrecht. 329–353.

Kelkar, V. K., B. K. Mishra, K. Srinivasa Rao, P. S. Goyal, and C. Manohar. 1991. Transition from a non-ionic to an ionic micelle. *Phys. Rev. A*. 44:8421–8424.

Kelkar, V. K., J. Narayanan, and C. Manohar. 1992. Structure factor for colloidal dispersions. use of exact potentials in random phase approximation. *Langmuir*. 8:2210–2214.

Malfois, M., F. Bonnete, L. Belloni, and A. Tardieu. 1996. A model of attractive interactions to account for fluid–fluid phase separation of protein solutions. *J. Chem. Phys*. 105:3290–3300.

Malkin, A., J. Yu, G. Kuznetsov, and A. McPherson. 1999. In situ atomic force microscopy studies of surface morphology, growth kinetics, defect structure and dissolution in macromolecular crystallization. *J. Crystal Growth*. 196:471–488.

Manohar, C., and V. K. Kelkar. 1992. Theory of colloidal systems: interactions and structure. *Langmuir*. 8:18–22.

Matsuda, S., T. Senda, S. Itoh, G. Kawano, M. Mizuno, and Y. Mitsui. 1989. New crystal form of recombinant murine interferon-beta. *J. Biol. Chem*. 264:13381–13382.

Molina-Bolivar, J. A., F. Galisteo-Gonzalez, and R. Hidalgo-Alvarez. 1997. Colloidal stability of protein–polymer systems: a possible explanation by hydration forces. *Phys. Rev. E*. 55:4522–4530.

Muschol, M., and F. Rosenberger. 1997. Liquid-liquid phase separation in supersaturated lysozyme solutions and associated precipitate formation/ crystallization. *J. Chem. Phys*. 107:1953–1962.

Muschol, M., and F. Rosenberger. 1995. Interactions in undersaturated and supersaturated lysozyme solutions: static and dynamic light scattering results. *J. Chem. Phys*. 103:10424–10432.

Neal, B. L., D. Asthagiri, O. D. Velev, A. M. Lenhoff, and E. W. Kaler. 1999. Why is the osmotic second virial coefficient related to protein crystallization? *J. Crystal Growth*. 196:377–387.

Orthaber, D., A. Bergmann, and O. Glatter. 2000. SAXS experiments on absolute scale with Kratky systems using water as a secondary standard. *J. Appl. Cryst*. 33:218–225.

Petsev, D. N., and P. G. Vekilov. 2000. Evidence for non-DLVO hydration interactions in solutions of the protein apoferritin. *Phys. Rev. Lett*. 84:1339–1342.

Price, W. S., F. Tsuchiya, and Y. Arata. 1999. Lysozyme aggregation and solution properties studied using PGSE NMR diffusion measurements. *J. Am. Chem. Soc*. 121:11503–11512.

Rosenbaum, D. F., and C. F. Zukoski. 1996. Protein interactions and crystallization. *J. Crystal Growth*. 169:752–758.

Rosenberger, F. 1996. Protein crystallization. *J. Crystal Growth*. 168: 40–54.

Rosenberger, F., P. G. Vekilov, M. Muschol, and B. R. Thomas. 1996. Nucleation and crystallization of globular proteins—what do we know and what is missing? *J. Crystal Growth*. 168:1–27.

San Biagio, P. L., and M. U. Palma. 1991. Spinodal lines and Flory-Huggins free energies for solutions of human hemoglobins HbS and HbA. *Biophys. J.* 60:508–512.

Skouri, M., J.-P. Munch, B. Lorber, R. Giege, and S. J. Candau. 1992. Interactions between lysozyme molecules under precrystallization conditions studied by light scattering. *J. Crystal Growth*. 122:14–20.

Steinhardt, J., and J. A. Reynolds. 1969. Multiple Equilibria in Proteins, Academic Press, New York.

Tanaka, S., M. Yamamoto, K. Ito, R. Hayakawa, and M. Ataka. 1997. Relation between the phase separation and the crystallization in protein solutions . *Phys. Rev. E.* 56:R67–R69.

Tanaka, S., M. Yamamoto, K. Kawashima, K. Ito, R. Hayakawa, and M. Ataka. 1996. Kinetic study on the early stage of the crystallization process of two forms of lysozyme crystals by photon correlation spectroscopy . *J. Crystal Growth*. 168:44–49.

Tanford, C., and R. Roxby. 1972. Interpretation of protein titration curves. Application to lysozyme. *Biochemistry*. 11:2192–2198.

Tardieu, A., A. Le Verge, M. Malfois, F. Bonnete, S. Finet, M. Reis-Kautt, and L. Belloni. 1999. Proteins in solution: from x-ray scattering intensities to interaction potentials. *J. Crystal Growth*. 196:193–203.

Tardieu, A., S. Finet, and F. Bonnete. 2001. Structure of macromolecular solutions that generate crystals. *J. Crystal Growth*. 232:1–9.

Thomson, J. A., P. Schurtenberger, G. M. Thurston, and G. B. Benedek. 1987. Binary liquid phase separation and critical phenomena in a protein/water solution. *Proc. Natl. Acad. Sci. USA*. 84:7079–7083.

Valstar, A., W. Brown, and M. Almgren. 1999. The lysozyme-sodium dodecyl sulfate system studied by dynamic and static light scattering. *Langmuir*. 15:2366–2374.

Vekilov, P. G., F. Rosenberger, H. Lin, and B. R. Thomas. 1999. Nonlinear dynamics of layer growth and consequences for protein crystal perfection. *J. Crystal Growth*. 196:261–275.

Velev, O. D., E. W. Kaler, and A. M. Lenhoff. 1998. Protein interactions in solution characterized by light and neutron scattering: comparison of lysozyme and chymotrypsinogen. *Biophys. J.* 75:2682–2697.

Verwey, E. J. W., and J. T. G. Overbeek. 1948. Theory of the Stability of Lyophobic Colloids. Elsevier, Amsterdam.

Wolde, P. R. T., and D. Frenkel. 1997. Enhancement of protein crystal nucleation by critical density fluctuations. *Science*. 277:1975–1978.

Zimm, B. H. 1948. The scattering of light and the radial distribution function of high polymer solutions. *J. Chem. Phys*. 16:1093–1099.